THE ANNALS OF "DUNAREA DE JOS" UNIVERSITY OF GALATI.
FASCICLE IX. METALLURGY AND MATERIALS SCIENCE
N^0. 2 – 2008, ISSN 1453 – 083X

AN ANALYTICAL PROCEDURE FOR THE PREDICTION OF THE STRESS-STRAIN STATE IN NOTCHES UNDER MULTIAXIAL FATIGUE

Nikolas PITATZIS[1], Alexander SAVAIDIS[2], Georgios SAVAIDIS[1]

[1] Aristotle University of Thessaloniki, Dept. of Mechanical Engineering, Greece
[2] National Technical University of Athens, Department of Mechanics, Greece
e-mail: pitatzis@auth.gr

ABSTRACT

This work presents an analytical procedure for estimating elastic-plastic stresses and strains in notched shafts subjected to synchronous non-proportional torsional and tensile cyclic loading. The specification of the equivalent stress concentration factor is firstly accomplished. Neuber's rule in conjunction with the assumed material law provides the relation between the applied loading and the equivalent stress and strain. Principal stresses and strains yield from the corresponding equivalent values incorporating Hencky's equations. The transformation of the principal stresses and strains to the appropriate coordinate system yields the final result. For the assessment of the analytical procedure, notch stress-strain results from several finite element analyses of an axisymmetric cylindrical shaft with a circumferential groove subjected to multiaxial synchronous fatigue loading are presented. A satisfactory agreement between the analytical and numerical results is observed.

KEYWORDS: Finite elements, Plasticity, Notches, Analytical model, Fatigue

1. Introduction

Engineering components often provide unavoidable local stress concentrations due to notches or other geometrical discontinuities. Such stress concentration sites yield intense cyclic plastic deformation under service loading, which may give rise to a drastic reduction in the operational lifetime of a structure. The understanding of the local stress-strain responses on the failure-critical areas and a thorough cognition into the damage evolution process are ultimate prerequisites to preserve structural safety in conjunction with design optimization.

Nowadays, extensive literature exists concerning approximate methods for computing notch stresses and strains. For the pure elastic case, the quantities of interest are the stress concentration factors, which describe the local stress amplification at a notch-root. Approximate and exact results for stress concentration factors can be found in many reference books [22, 25, 35]. Studies on this subject can be found in [8, 24, 40]. The corresponding elastic–plastic notch problems are, however, much more complex than those for the pure elastic case. For uniaxial loading, approximate methods have been proposed in [5, 9, 11, 17, 23, 27, 35, 36]. Applications of Neuber's rule to notch fatigue analysis have been presented in [34, 37]. Approximate methods for the estimation of multiaxial stress–strain have been developed in [1, 2, 5-7, 9, 10, 12-16, 38].

In our previous works [29-32] basic investigations dealing with the well-known kinematic hardening rule of Prager-Ziegler [26, 39] in conjunction with the von Mises yield criterion [19] were investigated. Prager-Zieler's kinematic hardening rule is capable to describe linear material hardening in a reliable way. Therefore, and due to its simplicity, it is implemented in all common commercial finite element programs. However, neither the material cyclic stress-strain curve, nor the hysteresis loop shapes that arise during the fatigue process can be described with good precision [18].

Especially in low cycle fatigue with high plastic strains, as well as in cases with variable amplitude cyclic loading a linear kinematic hardening model is not capable to provide a realistic transposition of the

yield surface within the whole stress spectrum. To overcome these obstacles, several improvements have been proposed during the last decades. One way to cope with these deficiencies is to apply multilayer [4] or multisurface [21] models. Thus, the curved stress-strain relations can be sufficiently approximated by means of multi-segment lines providing the desired accuracy.

In the present work, an approximate model [28, 32] will be used for computing the complete elastic–plastic notch stresses and strains. In order to verify the model, detailed elastic–plastic FE analyses for a cylindrical shaft with a circumferential notch are performed. The elastic–plastic material properties are described by the von Mises yield criterion [19] and the multilayer material model of Besseling [4]. Synchronous non-proportional cyclic tension/torsion loading with constant and variable amplitudes is applied to validate the accuracy of the results derived from the analytical model comparing them with the corresponding FE results.

2. Problem formulation

Consider an infinite and elastic-plastic cylindrical shaft with a circumferential groove as depicted in fig. 1.

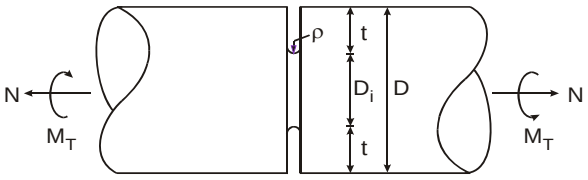

Fig. 1. *The infinite notched shaft*

Table 1 includes the geometrical dimensions of the cylindrical shaft under investigation.

Table 1. *Geometrical parameters in [mm]*

Shaft Diameter	Crucial Diameter	Notch Depth	Notch Radius
D	D_i	t	P
140	70	35	3

A tensile force N combined with a torsional moment M_T are applied on the notched shaft. For convenience, the nominal tensile stress S and the nominal shear stress T, instead of N and M_T are used as external loads in the analysis, which are related by

$$S = \frac{N}{\pi(D_i/2)^2}, \qquad T = \frac{2M_T}{\pi(D_i/2)^3}. \tag{1}$$

3. Approximation model

The origin of the analytical model goes back to the work of Savaidis et al [28, 32]. The model uses the same input as the well-known model of Hoffmann and Seeger [12-15] for *proportional* loading as starting point. Taking the material's stress-strain curve and the notch concentration factors for every individual loading as an input, two steps are performed.

Step 1: *Relationship between applied load and equivalent notch stress* σ_{eq} *and strain* ε_{eq}.

The elastic solution is based on the approximate uniaxial stress–strain relation for the equivalent quantities. The material law in conjunction with the elastic solution yields the relation between the applied external load and the equivalent stress, defined by the equation:

$$\varepsilon_{eq} = \frac{\sigma_{eq}}{E} F\left(\frac{\sigma_{eq}^e}{\sigma_{eq}}, K_p\right) \frac{E\varepsilon^*}{S^*}, \tag{2}$$

where the superscript 'e' denotes the elastic solution, F is a function of the ratio $\sigma_{eq}^e / \sigma_{eq}$ and the plastic limit load factor K_p, while S^* and ε^* are the modified nominal stress and strain respectively. In particular they are defined by

$$K_p = \frac{\sigma_u}{\sigma_y}, \quad S^* = \frac{\sigma_{eq}^e}{K_p}, \quad \varepsilon^* = g^{-1}\left(S^*\right), \tag{3}$$

in which σ_u is the ultimate limit load and σ_y is the load at yield initiation.

Step 2: *Derivation of the individual stress and strain components or principal stresses and strains from the equivalent stress* σ_{eq} *and strain* ε_{eq}.

For this, use is made of the yield criterion, flow rule and the boundary as well as the constraint conditions at the notch-root. The Prandtl-Reuss law yields

$$d\varepsilon_i^p = \frac{3}{2h}\frac{d\varepsilon_{eq}^p}{\sigma_{eq}} \cdot \sigma_i', \quad i = 1,2,3, \tag{4}$$

with the plastic tangent modulus $h = d\sigma_{eq} / d\varepsilon_{eq}^p$, while the Hencky's law results in

$$\varepsilon_i^p = \frac{3}{2}\frac{\varepsilon_{eq}^p}{\sigma_{eq}}\sigma_i'. \tag{5}$$

Assume that the directions of the principal stresses remain unchanged during loading, i.e., φ_i = const., then the following boundary and constraint conditions hold at the notch-root: σ_3=0, $\varepsilon_2/\varepsilon_1$=const. The output quantities are the notch stresses σ_{ij}=0, notch strains ε_{ij} or ε_i, and the directions of the principal stress axes characterized by the orientation angles φ_i.

The *non-proportional* loading can be classified into two different categories as illustrated in fig. 4. In the first loading category, both loading components are cyclic. In the second loading category, one

loading component is cyclic, while the other is kept constant. Three cases are distinguished according to fig. 2:

- Case I: Both components, S and T, are cyclic and $1 \geq S_a/T_a \geq 0.65$. This case corresponds to a large amplitude ratio S_a/T_a.
- Case II: S (or T) is constant while T (or S) is cyclic, and $0.05 \geq S_a/T_a \geq 0$ (or $0.05 \geq T_a/S_a \geq 0$). This case corresponds to a small amplitude ratio S_a/T_a (or T_a/S_a).
- Case III: Both components S and T are cyclic, and $0.65 \geq S_a/T_a \geq 0.05$. This case corresponds to a moderate amplitude ratio S_a/T_a.

With cases I, II and III, the complete range of the amplitude ratio S_a/T_a is covered.

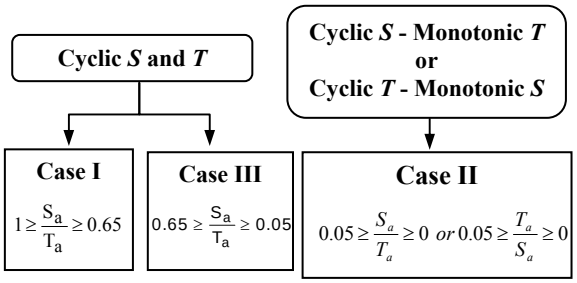

Fig. 2. *Load case classification within the framework of the analytical model*

Detailed description how to proceed within each case is given in [28, 32].

4. Finite elements

To verify the analytical procedure, various numerical analyses for a multiaxially loaded notched shaft have been performed. For its discretization 13120 solid elements have been applied. Each element consists of 20 nodes and 14 Gaussian points. The total number of nodes is 51677. The shaft has been divided up to 40 cylindrical segments, each having an angle θ=9^o. In the non-linear analysis, a full Newton-Raphson procedure [3] for all degrees of freedom has been applied. A section of the shaft is shown in fig. 3, whereby the element distribution is distinguished.

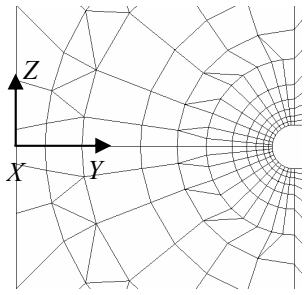

Fig. 3. *Mesh configuration*

The material law of the aluminum alloy Al5083 is considered. The experimentally determined values of the cyclic hardening coefficient K' and the cyclic hardening exponent n' amount to K' = 544 N/mm^2 and n' = 0.075, respectively. The elastic modulus E and Poisson's ratio v amount to E = 68000 N/mm^2 and v = 0.32, respectively.

5. Loading cases

Table 2 summarizes the non-proportional synchronous loading cases investigated here.

Table 2*. Loading cases under investigation*

Load case	C	S_m [N/mm^2]	T_a [N/mm^2]	S_{eq} [N/mm^2]
L1	0	0	225.630	390.8
L2	0.623	132.269	212.311	390.8
L3	1.000	195.402	195.402	390.8
L4	1.605	265.626	165.499	390.8
L5	5.000	369.275	73.855	390.8
L6	10.00	385.070	38.507	390.8
	D	T_m [N/mm^2]	S_a [N/mm^2]	S_{eq} [N/mm^2]
L7	0	0	390.804	390.8
L8	0.623	65.492	265.637	390.8
L9	1.000	195.402	195.402	390.8
L10	10.00	225.255	22.525	390.8

Two main loading categories are distinguished in Table 2: (a) cyclic fully reversed tension-compression combined with monotonic torsion, and (b) cyclic fully reversed torsion combined with monotonic tension. The mean value of the individual cyclic load component is kept zero in all cases.

For convenience, the ratio $c=S_m/T_a$ of the constant nominal normal stress S_m to the nominal shear stress amplitude T_a is used to describe the load situation. The ratio $d=T_m/S_a$ of the constant nominal shear stress T_m and the nominal normal stress amplitude S_a is also considered. The nominal equivalent stress S_{eq} is kept constant and larger than the value of the material flow stress σ_y in all loading cases.

Note that the monotonic loading component acts first on the notched shaft. When it reaches its pick value then the cyclic loading component is applied. Therefore, the attained phase difference between the two loading components is 90^o.

6. Results

Results derived from the finite element analyses and the analytical model are discussed in this section. For clarity, each result is specified with a code name; the first letter refers to the solution method (F for the

finite element procedure, A for the analytical procedure). The letter "L" follows, denoting loading. Next, a number (1 to 10) refers to each one of the ten loading cases presented herein.

The stabilized notch stress-strain curves will be considered in the following discussions of the results.

Figure 4 shows the τ_{yz}-γ_{yz} results for the loading case L2.

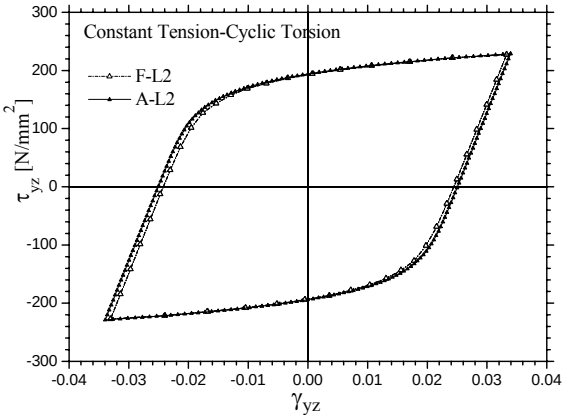

Fig. 4. *Comparison of the τ_{yz}-γ_{yz} hystereses determined by FE analysis and the analytical model for the loading case L2*

A very good agreement to both stress and strain results can be observed in that loading case as the two plotted stabilized τ_{yz}-γ_{yz} are almost identical.

Figure 5 shows the results for the loading cases L1 to L6, whereby the influence of the *c*-value on the stress-strain behavior is explored.

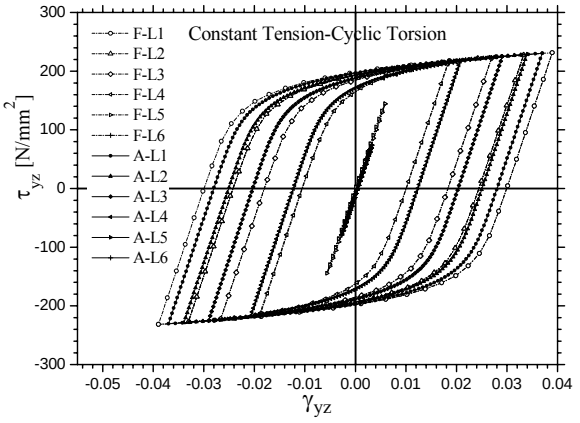

Fig. 5*. Comparison of τ_{yz}-γ_{yz} hystereses determined by FE analysis and the analytical model for the loading cases L1 to L6*

Thereby, the value of *c* increases from 0 (L1) to 10 (L6). In the cases of *c*=5 (L5) and *c*=10 (L6) with very low cyclic loads, the calculated plastic deformation is approximately zero. Therewith, the τ_{yz}-γ_{yz} response is nearly the same and it follows the Hooke's law. For *c*<1.6, where the shear plastic deformation attains significant values, (small) discrepancies between the finite element and the analytical model's results occur.

It must be noticed that the finite element method calculates erroneously a radial stress component at the notch root. This error results from the stress extrapolation from the inner element Gaussian points to the corner element nodes. Therefore, according to the finite element solution the material shows a stiffer attitude because of the presence of the radial stress component. Theoretically, no radial stress should exist at the very notch root, as correctly assumed in the analytical procedure's formulation. The value of this erroneous radial stress component increases with increasing plastic deformations. Therewith, the observed disagreement between the numerical and the analytical results becomes more evident for greater *c* values.

Figure 6 shows the normal stress-normal strain response (σ_z-ε_z) at the notch root for loading case L10. Herein, the results of the analytical solution as well as the ones from two finite element analyses are compared. Each finite element solution corresponds to a different mesh configuration. The solution indicated with the letter "F" in fig. 6 was determined with the finite element mesh described in section 4. Another coarser mesh configuration has been created including only 1360 elements and 6077 nodes, in order to explore the effect of the radial stress on the finite element results and on the σ_z-ε_z path. The letter 'C' in fig. 6 stands for the finite element solution where the coarse mesh version is applied.

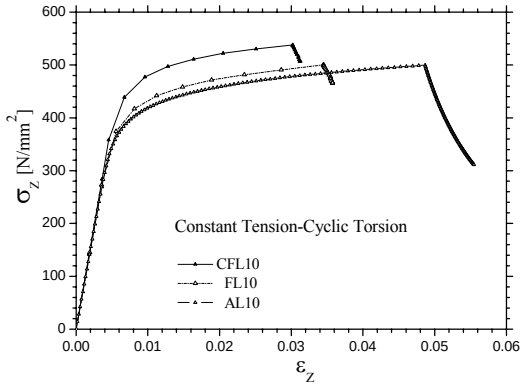

Fig. 6. *Comparison of σ_z-ε_z hystereses determined by FE analyses and the analytical model for the loading case L10*

A stiffer material response is regarded from the finite element solutions compared to the one derived from the analytical model. The finite element mesh refinement results in a subsequent increase in the number of integration points and therefore decreases the radial stress component value. That leads to a numerical solution where the material yields at lower normal stress values according to von Mises yield criterion. Nonetheless, the presence of a (erroneous)

radial stress component -even in the case of a finer mesh- yields results that differ from the ones derived from the analytical model.

The significant differences in the calculated normal strain are due to the assumption that the strain ratio $\varepsilon_2/\varepsilon_1$ should remain constant throughout the whole loading history according to the analytical model. This is valid for elastic stress-strain responses but not valid in cases where plastic strains are prevalent like in the loading cases under study.

The σ_z-ε_z diagram shown in fig. 7 incorporates results from the finite element and the analytical procedure implementation for several *d*-values.

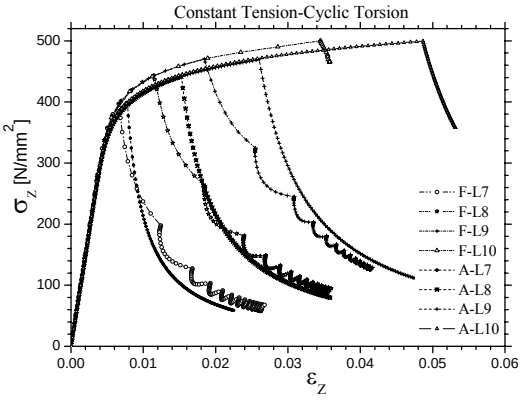

Fig. 7. *Comparison of the σ_z-ε_z hystereses determined by FE analyses and the analytical model for the loading cases L7 to L10*

As *d* increases successively from load case L7 up to L10, the observed differences to the calculated normal strain become more and more significant. This is due to the gradual increase of $\varepsilon_2/\varepsilon_1$ for increasing normal load values. This increase becomes prominent for the sharp notch investigated here because of the notch constraint.

7. Conclusions

An analytical procedure to evaluate the stress-strain response in notched components under synchronous nonproportional loading is assessed based on numerical results from finite element analyses for a circumferentially notched shaft subjected to synchronous non-proportional multiaxial fatigue loading consisting of cyclic and static load components. The following conclusions can be derived from the comparative analyses:

- A good agreement between the analytically and numerically determined shear stresses and shear strains has been observed even in loading cases with excessive plastic shear strain values.
- The application of a finite element mesh configuration that includes adequate number of nodes with high node density especially nearby the notch root is an indispensable prerequisite for a reliable finite element solution.
- The analytical model as far as the normal stress – normal strain path monitoring is concerned, achieves an acceptable description of the notch constraint.
- Deviations between the analytically and numerically calculated normal strains exist due to the assumption of a constant $\varepsilon_2/\varepsilon_1$-ratio within the framework of the analytical procedure, especially in loading cases causing pronounced plastic strains.

References

[1]. Amstutz H., Hoffmann M., Seeger T., 1988, *Kerbbeanspruchungen II – Mehrachsige Kerbbeanspruchungen im nichtlinearen Bereich bei proportional und nichtproportional wechselnder Belastung*, Heft 139, Forschungshefte Forschungs-kuratorium Maschinenbau e.V., Frankfurt, Germany.

[2]. Barkey M.E., Socie D.F., Hsia K.J., 1993, *A Yield Surface Approach to the Estimation of Notch Strains for Proportional and Nonproportional Cyclic Loading*, TAM Report No. 709-UILU ENG-93-6007, University of Illinois, Urbana-Champaign, USA.

[3]. Bathe K., 1996, *Finite Element Procedures*, Prentice Hall, New Jersey.

[4]. Besseling, J.F., 1958, A Theory of Elastic, Plastic, and Creep Deformations of an Initially Isotropic Material Showing Anisotropic Strain-Hardening Creep Recovery and Secondary Creep, J. Appl. Mech., pp. 529-536.

[5]. Dietmann H., 1968, *Berechnung der Fliesskurven von Bauelementen bei kleinen Verformungen*, readership thesis, University of Stuttgart, Germany.

[6]. Dowling N.E., Brose W.R., Wilson W.K., 1977, *Notched Member Fatigue Life Predictions by the Local Strain Approach in Fatigue under Complex Loading*, Advances in Engineering, 6, SAE, Warrendale, pp. 55–84.

[7]. Esderts A., Amstutz H., 1994, *Betriebsfestigkeit bei mehrachsiger Beanspruchung II*, Heft 188, Forschungshefte Forschungskuratorium Maschinenbau e.V., Frankfurt, Germany.

[8]. Filippini M., 2000, *Stress Gradient Calculations at Notches*, Int. J. Fatigue, 22, pp. 397–409.

[9]. Glinka G., 1985, *Energy Density Approach to Calculation of Inelastic Strain–Stress near Notches and Cracks*, Eng. Fract. Mech., 22, pp. 485–508.

[10]. Grubisic V., Sonsino C.M., 1982, *Influence of Local Strain Distribution on Low-Cycle Fatigue Behavior of Thick-Walled Structures*, ASTM-STP 770, pp. 612–629.

[11]. Hardrath H.F., Ohman H., 1951, *A Study of Elastic Plastic Stress Concentration Factors due to notches and fillets in plat plates*, Technical Note NACA TN 2566.

[12]. Hoffmann M., Seeger T., 1985, *A Generalized Method for Estimating Multiaxial Elastic–Plastic Notch Stresses and Strains*. Part 1 - Theory, J. Eng. Mater. Technol., 107, pp. 250-254.

[13]. Hoffmann M., Seeger T., 1985, *A Generalized Method for Estimating Multiaxial Elastic–Plastic Notch Stresses and Strains. Part 2 - Application and general discussion*, J. Eng. Mater. Technol., 107, pp. 255–260.

[14]. Hoffmann M., Seeger T., 1985, *Kerbbeanspruchungen I – Ermittlung und Beschreibung mehrachsiger Kerbbeanspruchungen im nichtlinearen Bereich,* Heft 115, Forschungshefte Forschungskuratorium Maschinenbau e.V., Frankfurt, Germany.

[15]. Hoffmann M., Seeger T., 1989, *Stress–Strain Analysis and Life Predictions of a Notched Shaft under Multiaxial Loading, Multiaxial Fatigue – Analysis and Experiments*, SAE AE-14, Warrendale, pp. 81–101.

[16]. Knop M., Jones R., Molent L, Wang C., 1999, *On the Glinka and Neuber methods for Calculating Notch Tip Strains under Cyclic Load Spectra*, Int. J. Fatigue, 22, pp. 743–755.

[17]. Kühnapfel K.F., 1976, *Kerbdehnungen und Kerbspannungen bei elasto-plastischer Beanspruchung; rechnerische Ermittlung, Vergleich mit Versuchsergebnissen*, phD-thesis, TH Aachen, Germany.

[18]. Lemaitre J., Chaboche J.L., 1990, *Mechanics of Solid Materials*, Cambridge University Press.

[19]. von Mises, R,. 1913, *Mechanik der festen Körper im plastisch-deformablen Zustand*, Nachr. Konigl. Ges. Wiss. Göttingen, math. phys., pp. 582-593.

[20]. Mowbray D.F., McConnelee J.E., 1073, *Applications of Finite Element Stress Analysis and Stress–Strain Properties in Determining Notch Fatigue Specimen Deformation and Life*, ASTM STP 519, pp. 151–169.

[21]. Mroz Z., 1967, *On the Description of Anisotropic Work Hardening*, J. Mech. Phys. Solids., 17, pp. 163-175.

[22]. Neuber H., 2001, Kerbspannungslehre, 4th edition, Springer-Verlag.

[23]. Neuber H., 1961, *Theory of Stress Concentration for Shear strained Prismatical Bodies with Arbitrary Nonlinear Stress–Strain Law,* J. Appl. Mech., 28, pp. 544–550.

[24]. Noda N.A., Takase Y., 1999, *Stress Concentration Formulae useful for any Shape of Notch in a Round Test Specimen under Tension and under Bending*, Fatigue Fract. Engng Mater. Struct., 22, pp.1071–1082.

[25]. Peterson R.E., 1974, The Stress Concentration Factors Handbook, John Wiley and Sons, New York.

[26]. Prager W., 1955, *The Theory of Plasticity: A Survey of Recent Achievements.* Proc. Inst. Mech. Engrs., 169, pp. 41-57.

[27]. Saal H., 1975, *Näherungsformeln für die Dehnformzahl*, Materialprüfung, 17, pp. 395- 398.

[28]. Savaidis A., 1994, *Finite-Element Untersuchungen und Entwicklung eines N€aherungsverfahrens zur Beschreibung mehrachsiger elastisch-plastischer Kerbbeanspruchungen bei synchroner nichtproportionaler zyklischer Belastung*, 52, Institut für Stahlbau und Werkstoffmechanik, TU Darmstadt, Germany.

[29]. Savaidis A., Savaidis G., Zhang Ch., 2001, *FE Fatigue Analysis of Notched Elastic-Plastic Shaft Under Multiaxial Loading Consisting of Constant and Cyclic Components*, Int. J. Fatigue, 23, pp. 303-315.

[30]. Savaidis A., Savaidis G., Zhang Ch., 2001, *Elastic-Plastic FE Analysis of a Notched Shaft Under Multiaxial Nonproportional Cyclic Loading,* Theor. Appl. Fract. Mech., 32, pp. 87-97.

[31]. Savaidis A., Savaidis G., Zhang Ch., 2002, *Numerical Analysis of Notched Elastic-Plastic Structures Under Multiaxial Variable Amplitude Loading*, Computers and Structures, 80, pp. 1907-1918.

[32]. Savaidis A., Savaidis G., Zhang Ch., 2003, *Approximate Elastic-Plastic Analysis of a Notched Bar Under Tensile and Torsional Fatigue*, Theor. Appl. Fract. Mech., 40, pp. 85-96.

[33]. Seeger T., Beste A., 1977, *Zur Weiterentwicklung von Näherungsformeln für die Berechnung von Kerbbeanspruchungen im elastisch-plastischen Bereich*, VDI Verlag, Reihe 18, No 2, pp. 1–56.

[34]. Seeger T., Heuler P., 1980, *Generalized Application of Neuber's Rule*, J. Test. Eval., 8, pp. 199–204.

[35]. Sih G.C. (Ed.), 1978, *Stress Analysis of Notch Problems, Mechanics of Fracture*, 5, Noordhoff International Publishing, Leyden.

[36]. Stowell E.Z., 1950, *Stress and Strain Concentration at a Circular Hole in an Infinite Plate*, Technical Note NACA TN 2073.

[37]. Topper T.H., Wetzel R.M., Morrow J.D., 1969, *Neuber's Rule Applied to Fatigue of Notched Specimens*, J. Mater., 1, pp. 200–209.

[38]. Walker E.K., 1977, *Multiaxial Stress–Strain Approximations for Notch Fatigue*, J. Test. Eval., 5, pp. 106–113.

[39]. Ziegler H., 1959, A *Modification of Prager's Hardening Rule.* Quart. Appl. Math., 17, pp. 55-60.

[40]. Zheng M., Niemi E., 1997, *Analysis of the Stress Concentration Factor for a Shallow Notch by the Slip-Line Field Method*, Int. J. Fatigue, 19, pp. 191–194.